# EPR of $Gd^{3+}$-doped single crystals of $LiY_{1-x}Yb_xF_4$

Lucjan E. Misiak* and Sushil K. Misra
*Physics Department, Concordia University, 1455 de Maisonneuve Blvd. West, Montreal, Quebec, Canada H3G 1M8*

Pawel Mikolajczak
*Department of Experimental Physics, Maria Curie-Sklodowska University, 20-031 Lublin, Poland*
(Received 28 March 1988)

Extensive $X$-band EPR measurements have been carried out on $Gd^{3+}$-doped single crystals of $LiY_{1-x}Yb_xF_4$ ($x=0.0$, 0.1, 0.2, 0.3, 0.4, 0.6, 0.8, 1.0), covering the temperature range 4.2–290 K. The spin-Hamiltonian parameters (SHP) are evaluated by the use of a rigorous least-squares fitting procedure. The systematics of the SHP are studied both as functions of $x$ and of temperature. Newman's superposition model has been applied to the calculation of SHP; it is found that the calculated values agree quite well with the experimental values, provided that one considers minor distortions of the positions of the eight fluorine ions surrounding the $Gd^{3+}$ ion. The temperature variation of SHP has been explained to be predominantly due to spin-phonon interaction and partially due to thermal expansion of the crystal lattice. Finally, the average $Gd^{3+}$-$Yb^{3+}$ exchange interaction, averaged over the nearest and next-nearest neighbors, has been estimated, in $LiY_{0.9}Yb_{0.1}F_4$, to be $3.8\pm2.5$ GHz, as found by the application of the molecular-field model using the $g$ shift from the isostructural diamagnetic host, $LiYF_4$, at liquid-helium temperature.

## I. INTRODUCTION

$LiYF_4$ and $LiY_{1-x}Yb_xF_4$ crystals have been used, respectively, as laser materials,[1] and as materials to convert infrared excitation to green emission.[2] $X$-band EPR measurements on single crystals of $Gd^{3+}$-doped $LiYF_4$ and $LiYbF_4$ have been previously reported by Vaills *et al.*[3] and by Misra *et al.*[4] Vaills *et al.*[3] confined their measurements to room temperature, and calculated the values of the spin-Hamiltonian parameters within the frameworks of the point-charge and superposition models. Misra *et al.*[4] extended these measurements down to liquid-helium temperatures, and evaluated the spin-Hamiltonian parameters (SHP) using a rigorous least-squares procedure.[5] They estimated the $Gd^{3+}$-$Yb^{3+}$ exchange interaction at room temperature using the $Gd^{3+}$ $g$ shift in $LiYbF_4$ from that in $LiYF_4$.

$Gd^{3+}$-doped $LiY_{1-x}Yb_xF_4$ crystals are interesting hosts for the study of magnetic interaction of $Gd^{3+}$ ion with its environment. Paramagnetic surroundings of $Gd^{3+}$ ion can be varied, while preserving the tetragonal symmetry, by replacing a certain fraction of $Y^{3+}$ ions by $Yb^{3+}$ ions in the diamagnetic host lattice of $LiYF_4$. These crystals are expected to have tetragonal structure, similar to that of $LiYF_4$, or $LiYbF_4$, crystals. Since the $Y^{3+}$ and $Yb^{3+}$ ions are trivalent, no charge compensation occurs when the substituting trivalent $Gd^{3+}$ ions are introduced in these crystals.

It is the purpose of the present paper to extend the previously reported $X$-band EPR studies on $Gd^{3+}$-doped $LiYF_4$ and $LiYbF_4$ single crystals to the mixed single crystals of $LiY_{1-x}Yb_xF_4$, with $x=0.0$, 0.1, 0.2, 0.3, 0.4, 0.6, 0.8, and 1.0. The spin-Hamiltonian parameters are, here, evaluated using a rigorous least-squares fitting procedure[5] in which all resonant EPR line positions recorded for several orientations of the external magnetic field are simultaneously fitted. The systematics of these SHP are studied as a function of $x$, representing the proportion of $Yb^{3+}$ ions present in these crystals. As well, the superposition model of Newman[6–8] is applied to the calculation of SHP; in particular, the dependences of the intrinsic parameters $\bar{b}_2$ and $\bar{b}_4$ upon temperature are studied. In addition, the systematics of $\bar{b}_2$ as a function of $x$ is investigated. The temperature dependence of the parameter $b_2^0$ is accounted for to be due to spin-phonon interaction and thermal expansion of the crystal lattice. Finally, for $LiY_{0.9}Yb_{0.1}F_4$, the only mixed crystal for which well-resolved EPR spectra can be recorded down to liquid-helium temperature, exchange interaction constant between the impurity paramagnetic ion $Gd^{3+}$ and the host paramagnetic ion $Yb^{3+}$ is estimated, using the shift of the $Gd^{3+}$ $g$ value in this host lattice from that in the isostructural diamagnetic host lattice of $LiYF_4$, taking into account the magnetization of the $Yb^{3+}$ lattice at liquid-helium temperature.

Section II deals with sample preparation and crystal structure of $LiY_{1-x}Yb_xF_4$ samples, while details of the experimental arrangement are given in Sec. III. Evaluation of SHP is described in Sec. IV. Details of the behavior of the zero-field splitting as functions of $x$ and of temperature, and application of the superposition model to the calculation of $Gd^{3+}$ SHP in $LiY_{1-x}Yb_xF_4$ hosts are described in Secs. V and VI, respectively. Temperature variation of SHP and evaluation of the $Gd^{3+}$-$Yb^{3+}$ exchange interaction in $LiY_{0.9}Yb_{0.1}F_4$ host crystals are presented in Secs. VII and VIII, respectively. Concluding remarks are made in Sec. IX.

 

## II. SAMPLE PREPARATION AND CRYSTAL STRUCTURE

Mixed single crystals of $LiY_{1-x}Yb_xF_4$, to which 0.3 mol. % $GdF_3$ was added, were grown by the Bridgman-Stockbarger method.[9] $LiYF_4$ and $LiYbF_4$ crystals have the Scheelite (tetragonal) structure with space-group classification $I4_1/a$.[10,11] The unit cell of $LiYF_4$ has the dimensions $a=5.167\pm0.003$ Å, $c=10.735\pm0.003$ Å,[9] while for $LiYbF_4$ $a=5.1335\pm0.0002$ Å and $c=10.588\pm0.002$ Å.[11] Since the values of $a$ and $c$ and the distances of the rare-earth metal in $LiYF_4$ and $LiYbF_4$ are quite close to each other, it is assumed that $LiY_{1-x}Yb_xF_4$ crystals also have the Scheelite structure, with the $a$ and $c$ dimensions scaled in the proportion of $x$ from those for $LiYF_4$ and $LiYbF_4$, using Vegard's law.[12–14]

## III. EXPERIMENTAL DETAILS

### A. Apparatus

EPR spectra were recorded on an $X$-band spectrometer model SE/X-28B, manufactured by Polytechnic School of Wroclaw, Poland, equipped with 100-kHz modulation and a maximum available microwave power of 100 mW. The 100-kHz modulation was mounted inside a $TE_{102}$ resonant cavity. The spectrometer could detect a minimum of $5\times10^{10}$ spins, characterized by a linewidth of 1 G (half width at half maximum of the absorption line), with a 1-s time constant. The external magnetic-field intensity was measured by a RADIOPAN NMR magnetometer (model MJ 110R), with a precision of 0.1 G. The crystal sample was placed inside a plexiglass holder, so that it could be rotated in a vertical plane, while the magnetic field was rotated in the horizontal plane. For measurements at low temperatures, a liquid-helium cryostat, with a temperature stability of $\pm0.1$ K below 77 K and of $\pm0.2$ between 77 and 300 K, was used. The microwave power was reduced appropriately at liquid-helium temperatures, in order to prevent saturation of $Gd^{3+}$ EPR lines.

### B. EPR spectra

The angular variations of spectra in any $Gd^{3+}$-doped $LiY_{1-x}Yb_xF_4$ single crystal were found to be similar to those in the $LiYF_4$ host crystal, described in Ref. 3. The features of the angular variation of spectra did not change with temperature, except that the EPR lines broadened in the hosts with higher concentrations of $Yb^{3+}$, due to the interaction of $Gd^{3+}$ guest with the $Yb^{3+}$ host ions, as the temperature was lowered, such that below certain temperatures, depending on $x$, well-resolved spectra could not be recorded. Clearly resolved EPR spectra could be recorded below room temperature down to liquid-helium temperatures (LHT) for samples with $x=0.0$ and $x=0.1$, down to 40 K for $x=0.2$, down to 100 K for $x=0.3$, down to 175 K for $x=0.4$; the remaining hosts did not yield clearly resolved EPR spectra even at temperatures much higher than liquid-nitrogen temperature (LNT). Resolved superhyperfine structure (SHFS) due to the nearest-neighbor fluorine nuclei was not visible in any $LiY_{1-x}Yb_xF_4$ crystal at any temperature.

For the orientation of the external magnetic field in the $ZX$ plane, a $\pi$ repetitive pattern, while in the $XY$ plane a $\pi/2$ repetitive pattern, was found for all the host crystals; these are exhibited in Figs. 1 and 2 for $LiY_{0.6}Yb_{0.4}F_4$ and $LiYF_4$ hosts, respectively.

### C. Linewidths

EPR linewidths for $Gd^{3+}$ ions in the $LiYF_4$ crystal were found to be $30\pm2$ G for all lines for the magnetic-field orientation along the $Z$ and $X$ axes at room temperature. When the temperature was lowered to 4.2 K, the linewidths increased slightly to $33\pm2$ G. In $LiY_{0.9}Yb_{0.1}F_4$ crystal the linewidths were very temperature dependent: 40–60 G at room temperature, 50–70 G at LNT, and 150–200 G at LHT. For the $LiY_{0.6}Yb_{0.4}F_4$ host the linewidths were 100–150 G at room temperature for the various transitions; these increased to 150–200 G at 170 K. All the lines in the $LiY_{0.6}Yb_{0.4}F_4$ crystal were well resolved down to $\sim170$ K, while at 40 K, for $\mathbf{H}\|\hat{\mathbf{X}}$, only the two highest-field lines could be observed, having

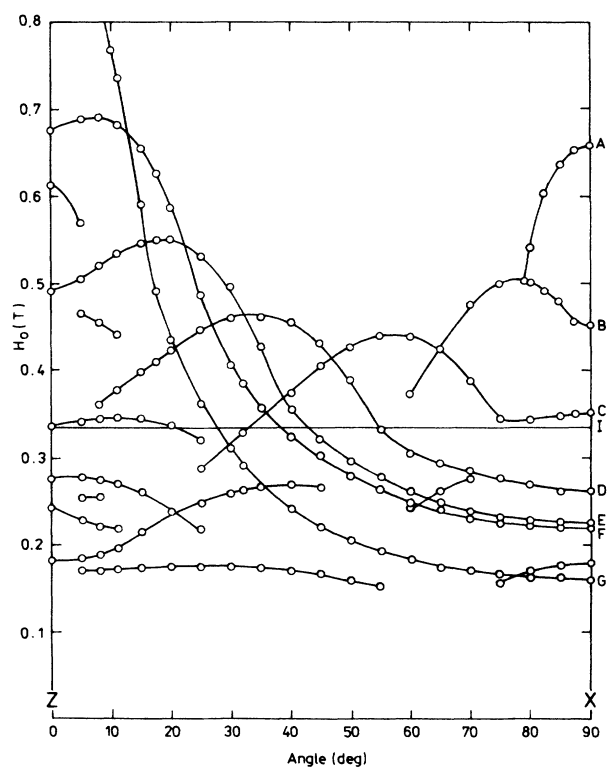


FIG. 1. Angular variation of $X$-band EPR line positions observed at room temperature for the $Gd^{3+}$-doped $LiY_{0.6}Yb_{0.4}F_4$ single crystal for the orientation of the external magnetic field in the $ZX$ plane. The various allowed transitions ($\Delta M=\pm1$) have been indicated as follows: $A$ $(-\frac{5}{2}\leftrightarrow-\frac{7}{2})$, $B$ $(-\frac{3}{2}\leftrightarrow-\frac{5}{2})$, $C$ $(-\frac{1}{2}\leftrightarrow-\frac{3}{2})$, $D$ $(\frac{1}{2}\leftrightarrow-\frac{1}{2})$, $E$ $(\frac{3}{2}\leftrightarrow\frac{1}{2})$, $F$ $(\frac{5}{2}\leftrightarrow\frac{3}{2})$, $G$ $(\frac{7}{2}\leftrightarrow\frac{5}{2})$, $I$ [diphenylpicrylhydrazyl (DPPH)]. At low fields some forbidden transitions ($\Delta M\neq\pm1$) are also observed, not shown here. The continuous lines connect data points belonging to the same transitions.

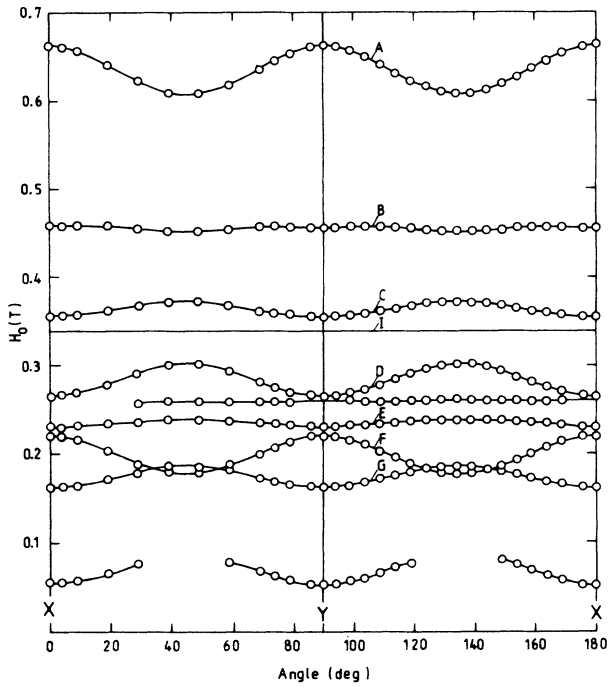


FIG. 2. Angular variation of $X$-band EPR line positions observed at room temperature for the $Gd^{3+}$-doped $LiYF_4$ single crystal for the orientation of the external magnetic field in the $XY$ plane. The various allowed transitions ($\Delta M=\pm 1$) have been indicated as follows: $A$ $(-\frac{5}{2}\leftrightarrow-\frac{7}{2})$, $B$ $(-\frac{3}{2}\leftrightarrow-\frac{5}{2})$, $C$ $(-\frac{1}{2}\leftrightarrow-\frac{3}{2})$, $D$ $(\frac{1}{2}\leftrightarrow-\frac{1}{2})$, $E$ $(\frac{3}{2}\leftrightarrow\frac{1}{2})$, $F$ $(\frac{5}{2}\leftrightarrow\frac{3}{2})$, $G$ $(\frac{7}{2}\leftrightarrow\frac{5}{2})$, $I$ (DPPH). At low fields some forbidden transitions ($\Delta M\neq\pm 1$) are also observed. The continuous lines connect data points belonging to the same transitions.

widths of about 500 G. (No observation were made for $\mathbf{H}\|\hat{\mathbf{Z}}$ at this temperature.) Below 40 K no clearly resolved lines could be observed in this crystal, even for $\mathbf{H}\|\hat{\mathbf{X}}$. (These linewidths are expressed in ranges, since they depend on the orientation and magnitude of the magnetic field.) The different temperature behaviors of $Gd^{3+}$ linewidths in $LiY_{1-x}Yb_xF_4$ hosts for different $x$, are obviously strongly dependent upon $x$, the fraction of $Yb^{3+}$ host ions present. The $Yb^{3+}$ ions affect the linewidths by dipole-dipole interaction with $Gd^{3+}$ ion. (Detailed interpretation of the linewidth behavior will be presented in a forthcoming publication.)

## IV. SPIN-HAMILTONIAN PARAMETERS

### A. Spin Hamiltonian

The spin Hamiltonian, characterizing $Gd^{3+}$ ion in $LiY_{1-x}Yb_xF_4$, substituting $Y^{3+}$, or the $Yb^{3+}$ ion, occupying the $S_4$ site, can be expressed as

$$\mathcal{H}=\mathcal{H}^r+\mathcal{H}^i\ , \tag{4.1}$$

where

$$\mathcal{H}^r=\mu_B\mathbf{H}\cdot\tilde{g}\cdot\mathbf{S}+\tfrac{1}{3}b_2^0O_2^0+\tfrac{1}{60}(b_4^0O_4^0+b_4^4O_4^4)+\tfrac{1}{1260}(b_6^0O_6^0+b_6^4O_6^4) \tag{4.2}$$

and

$$\mathcal{H}^i=\tfrac{1}{60}b_4^{-4}O_4^{-4}+\tfrac{1}{1260}b_6^{-4}O_6^{-4}\ . \tag{4.3}$$

In Eq. (4.2), $\mathbf{H}$ describes the external magnetic field intensity. In Eqs. (4.2) and (4.3), the $O_l^{\pm|m|}$ are spin operators, as defined by Abragm and Bleaney;[15] in particular, the matrix elements of $O_l^{+|m|}$ are real, while those of $O_l^{-|m|}$ are imaginary. As discussed by Vishwamittar and Puri,[16] the imaginary terms described by $\mathcal{H}^i$ can be ignored, thus approximating $\mathcal{H}\approx\mathcal{H}^r$, which is appropriate to $D_{2d}$ site symmetry. The ideal $D_{2d}$ symmetry corresponds to the case $\chi_1=\chi_2=0$; where $\chi_1$ and $\chi_2$ are the angles characterizing the projections of $F^-$ ligands in the $ab$ plane[16] (see Fig. 3). For $LiYF_4$,[16] $\chi_1=1°30'$ and $\chi_2=-2°29'$, while for $LiYbF_4$, $\chi_1=1°42'$ and $\chi_2=-2°49'$, as calculated using the crystal structure data for $LiYF_4$ and $LiYbF_4$. These angles are very small, thus justifying neglect of $\mathcal{H}^i$. The magnetic $Z$, $X$, and $Y$ axes, used in Eqs. (4.1)–(4.3), are defined to be those directions of the external magnetic field for which the extrema of overall splitting of EPR lines occur; the direction of the largest extremum defines the $Z$ axis, the direction of the next-largest extremum defines the $X$ axis, while the direction of the third-largest extremum defines the $Y$ axis. The magnetic $Z$ axis is found to be parallel to the crystal axis $c$. The orientation of the external magnetic field in the $ab$ plane for which the maximum splitting of EPR lines is observed, then, determines the magnetic $X$ axis; it is deduced to lie at $34°30'\pm 30'$ from the $a$ axis in the $ab$ plane.

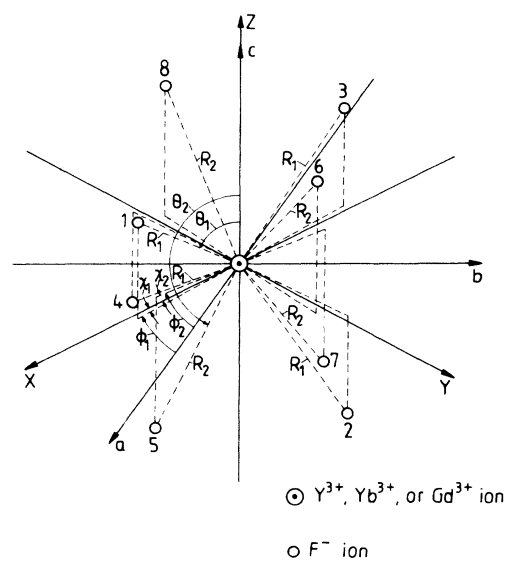


FIG. 3. Positions of $F^-$ ligand ions around the rare-earth ion in $LiY_{1-x}Yb_xF_4$ hosts. $X$, $Y$, and $Z$ denote the axes of the $b_2^m$ tensor, whereas $a$, $b$, and $c$ denote the crystal axes. The ligands 1–4 are at the same distance ($R_1$), while the ligands 5–8 are at the same distance ($R_2$), from the rare-earth ion. The $F^-$ ligands (1,3) and (5,7) have the polar angles $\theta_1$ and $\theta_2$, respectively, whereas the $F^-$ ligands (2,4) and (6,8) have the polar angles $\pi-\theta_1$ and $\pi-\theta_2$, respectively. The azimuthal angles for $i=1$–4 and 5–8 ligands are $\phi_1+(i-1)\pi/2$ and $\phi_2+(i-5)\pi/2$, respectively.

### B. Evaluation of spin-Hamiltonian parameters (SHP)

SHP were evaluated rigorously, using a least-squares-fitting (LSF) procedure,[5] fitting simultaneously all resonant line positions observed for **H** in the $ZX$ plane for all the $LiY_{1-x}Yb_xF_4$ host crystals. This meant evaluation of seven SHP: $g_{zz}$, $g_{xx}$, $b_2^0$, $b_4^m$, and $b_6^m$ ($m=0,4$), from a simultaneous fit of more than one-hundred line positions in each case. The relative signs of the parameters are correctly determined by the LFS procedure. The absolute signs of all SHP can, then, be determined from the knowledge of the absolute sign of $b_2^0$. The intensity of the highest-field lines relative to that of the lowest-field lines for $\mathbf{H}\|\hat{\mathbf{Z}}$ was found to decrease at liquid-helium temperature from that at room temperature for the $LiY_{0.9}Yb_{0.1}F_4$ host. This indicates that the absolute sign of $b_2^0$ is negative.[15] (The negative sign for $b_2^0$ has, thus, been assumed for all the other $LiY_{1-x}Yb_xF_4$ hosts, as well.) Figure 4 exhibits the temperature dependence of SHP for $LiY_{0.9}Yb_{0.1}F_4$, while Tables I–IV list the values of SHP for all the cases. It should be noted that the values of $b_6^0$ and $b_6^4$ were found to be practically zero, within experimental errors, for all the hosts. The temperature dependence of all the SHP has been found to be nonlinear in all the hosts; the absolute values of the parameters are, generally, found to increase with decreasing temperature. As for the dependences of the various SHP on the mole fraction $x$, the following is noted. The magnitudes of the parameters do not change much with $x$; these changes being 0.2, 18, and 5 % for $b_2^0$, $b_4^0$, and $b_4^4$, respectively. They are probably caused by lattice distortion, since the $Y^{3+}$ and $Yb^{3+}$ ions have unequal radii. Figure 5 exhibits temperature variation of $g_{zz}$ and $g_{xx}$ in the temperature range 4.2–296 K for $LiY_{0.9}Yb_{0.1}F_4$. In all the host crystals, both the $g_{zz}$ and $g_{xx}$ values decrease monotonically as the temperature is decreased from the room temperature, i.e., the $g$ shifts are negative (antiferromagnetic). The same result was found by Mehran *et al.*[17] in $Gd^{3+}$-doped $EuAsO_4$ and $EuVO_4$ crystals.

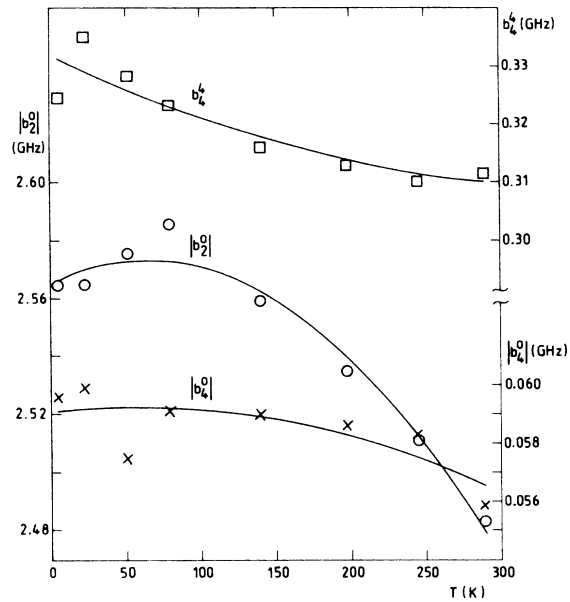


FIG. 4. Variation of the spin-Hamiltonian parameters as functions of temperature for $LiY_{0.9}Yb_{0.1}F_4$ crystal. The ○, ×, and □ represent the values of $|b_2^0|$, $|b_4^0|$, and $b_4^4$, respectively. Different parameters are characterized by different scales.

The values of the parameter $\alpha$, which determines the admixture of the excited state $^6P_{7/2}$ into the ground state $^8S_{7/2}$, are also included in Tables I–IV for all the hosts, at various temperatures. $\alpha$ is determined from the relation[18]

$$g=(1-\alpha^2)g_s+\alpha^2 g_p \ . \tag{4.4}$$

In Eq. (4.4), $g_s$ ($=2.0023$) and $g_p$ ($=1.716$) are, respectively, Lande's factors for $Gd^{3+}$ in the ground and first-excited states, while $g$ represents the average of $g_{zz}$ and

TABLE I. Values of SHP for $Gd^{3+}$-doped $LiYF_4$ at various temperatures. The parameters $b_l^m$ are expressed in GHz, while $g_{zz}$ and $g_{xx}$ are dimensionless, $n$ represents the total number of line positions simultaneously fitted to evaluate the parameters. $\chi^2 \equiv \sum_j (|\Delta E_j| - h\nu_j)^2$, where $\Delta E_j$ is the calculated difference in the energy levels participating in resonance for the $j$th line position, $\nu_j$ is the corresponding klystron frequency, and $h$ is Planck's constant. $\chi^2$ is expressed in $GHz^2$. $\alpha$ is the coefficient that represents the admixture of $^6P_{7/2}$ state in the $^8S_{7/2}$ state, as given by Eq. (4.4).

| $T$ (K) | 289 | 245 | 198 | 140 | 79 | 51 | 22 | 4.2 |
|---|---|---|---|---|---|---|---|---|
| $g_{zz}$ | 1.9901±0.0025 | 1.9903 | 1.9929 | 1.9911 | 1.9913 | 1.9915 | 1.9911 | 1.9900 |
| $g_{xx}$ | 1.9908±0.0025 | 1.9906 | 1.9920 | 1.9904 | 1.9914 | 1.9903 | 1.9920 | 1.9897 |
| $b_2^0$ | −2.4863±0.0085 | −2.5149 | −2.5426 | −2.5711 | −2.5918 | −2.5990 | −2.6010 | −2.6002 |
| $b_4^0$ | −0.0578±0.0015 | −0.0580 | −0.0585 | −0.0590 | −0.0596 | −0.0595 | −0.0594 | −0.0600 |
| $b_4^4$ | 0.3047±0.0046 | 0.3073 | 0.3107 | 0.3129 | 0.3143 | 0.3135 | 0.3130 | 0.3150 |
| $b_6^0$ | −0.0008±0.0037 | −0.0004 | −0.0003 | −0.0004 | −0.0004 | −0.0009 | −0.0002 | 0.0000 |
| $b_6^4$ | 0.0017±0.0095 | −0.0024 | 0.0001 | 0.0012 | −0.0002 | 0.0099 | 0.0069 | −0.0046 |
| $n$ | 106 | 106 | 106 | 106 | 106 | 84 | 105 | 113 |
| $\chi^2$ | 0.0391 | 0.0127 | 0.0268 | 0.0282 | 0.0350 | 0.1362 | 0.1791 | 0.0470 |
| $\alpha$ | 0.20 ±0.04 | 0.20 | 0.19 | 0.20 | 0.20 | 0.20 | 0.19 | 0.21 |

TABLE II. Values of SHP for $Gd^{3+}$-doped $LiY_{0.9}Yb_{0.1}F_4$. For notations see the caption of Table I.

| $T$ (K) | 289 | 245 | 198 | 140 | 79 | 51 | 22 | 4.2 |
|---|---|---|---|---|---|---|---|---|
| $g_{zz}$ | 1.9882±0.0030 | 1.9871 | 1.9855 | 1.9829 | 1.9868 | 1.9792±0.0040 | 1.9653 | 1.9661 |
| $g_{xx}$ | 1.9920±0.0030 | 1.9924 | 1.9933 | 1.9904 | 1.9927 | 1.9879±0.0040 | 1.9747 | 1.9757 |
| $b_2^0$ | −2.4830±0.0125 | −2.5108 | −2.5348 | −2.5591 | −2.5856 | −2.5753±0.0145 | −2.5647 | −2.5644 |
| $b_4^0$ | −0.0559±0.0020 | −0.0583 | −0.0586 | −0.0590 | −0.0591 | −0.0575±0.0030 | −0.0599 | −0.0596 |
| $b_4^4$ | 0.3114±0.0055 | 0.3101 | 0.3129 | 0.3158 | 0.3236 | 0.3285±0.0075 | 0.3352 | 0.3245 |
| $b_6^0$ | 0.0009±0.0055 | −0.0012 | −0.0009 | −0.0014 | −0.0009 | −0.0010±0.0075 | −0.0055 | −0.0038 |
| $b_6^4$ | −0.0057±0.0105 | −0.0094 | −0.0095 | −0.0107 | −0.0105 | −0.0259±0.0145 | −0.0091 | −0.0134 |
| $n$ | 107 | 107 | 108 | 105 | 104 | 104 | 93 | 92 |
| $\chi^2$ | 0.0622 | 0.0749 | 0.0943 | 0.1068 | 0.0893 | 0.1364 | 0.2021 | 0.2624 |
| $\alpha$ | 0.21 ±0.05 | 0.21 | 0.21 | 0.23 | 0.21 | 0.25 ±0.05 | 0.33 | 0.33 |

$g_{xx}$. It is found that this admixture increases with decreasing temperature for $LiY_{1-x}Yb_xF_4$ ($x \neq 1$) crystals, whereas for $LiYF_4$ its value is practically independent of temperature.

As for the temperature dependence of SHP, the parameters $b_2^0$, $b_4^0$, and $b_4^4$ are found to fit reasonably well, in the temperature range 4.2 K $< T <$ 300 K, to the quadratic function, $a + bT + cT^2$, for both the $LiYF_4$ and $LiY_{0.9}Yb_{0.1}F_4$ hosts, the only hosts for which well-resolved EPR spectra can be observed down to liquid-helium temperature. The values of the constants $a$, $b$, $c$, and the corresponding $\chi^2$ values for the various parameters are listed in Table V. A quadratic temperature dependence of $b_l^m$ was also observed by Low and Zusman[19] for $Gd^{3+}$-doped $LaAlO_3$ in the temperature range 20 K $< T <$ 300 K. According to them, the temperature dependence is due mainly to the changes in the crystal field. One expresses $b_2^0 = AV_{ax}(1 + BV_{ax})$, where $V_{ax}$ is the axial crystal-field strength, and $A$ and $B$ are complicated constants depending on a number of mechanisms; in particular, the spin-orbit coupling, the spin-spin interaction, and the energy separation of the $Gd^{3+}$ excited states from the ground state. The constants $A$ and $B$ do not depend significantly upon the temperature.[19] Thus, the temperature dependence of $b_l^m$ is mainly caused by the changes in $V_{ax}$, the axial crystal field. In order to explain the quadratic temperature dependence of $b_l^m$, $V_{ax}$ is, then, expected to be predominantly linear in the temperature range 4.2–300 K.

## V. ZERO-FIELD SPLITTING

It is interesting to study the dependence of $Gd^{3+}$ zero-field splitting in the $LiY_{1-x}Yb_xF_4$ hosts on temperature ($T$) and on the mole fraction ($x$). To this end, the eigenvalues of the spin-Hamiltonian matrix were calculated for $\mathbf{H}=0$ for the various host crystals. The overall zero-field splittings were then separately least-squares fitted to polynomials up to second power in $x$ and in $T$. Satisfactory fits were found to these quadratic polynomials. The results are as follows.

### A. Dependence on temperature

The zero-field splitting $\Delta E$ of $Gd^{3+}$ in $LiYF_4$ and $LiY_{0.9}Yb_{0.1}F_4$ hosts, the only crystals in which well-resolved spectra could be observed down to liquid-helium temperature, can be fitted, in the temperature range 4.2 K $< T <$ 300 K, to the following quadratic function:

TABLE III. Values of SHP for $Gd^{3+}$-doped $LiY_{1-x}Yb_xF_4$ ($x = 0.2, 0.3$). For notations see the caption of Table I.

| | $LiY_{0.8}Yb_{0.2}F_4$ | | | | $LiY_{0.7}Yb_{0.3}F_4$ | | | |
|---|---|---|---|---|---|---|---|---|
| $T$ (K) | 296 | 198 | 79 | 40 | 289 | 198 | 140 | 100 |
| $g_{zz}$ | 1.9810±0.0045 | 1.9788 | 1.9729 | 1.9597 | 1.9877 | 1.9857 | 1.9802 | 1.9699 |
| $g_{xx}$ | 1.9897±0.0045 | 1.9878 | 1.9880 | 1.9780 | 1.9913 | 1.9911 | 1.9902 | 1.9863 |
| $b_2^0$ | −2.4653±0.0145 | −2.5161 | −2.5575 | −2.5410 | −2.4805 | −2.5243 | −2.5486 | −2.5463 |
| $b_4^0$ | −0.0599±0.0030 | −0.0598 | −0.0588 | −0.0541 | −0.0582 | −0.0595 | −0.0616 | −0.0608 |
| $b_4^4$ | 0.3148±0.0075 | 0.3185 | 0.3337 | 0.3470 | 0.3158 | 0.3185 | 0.3341 | 0.3361 |
| $b_6^0$ | −0.0016±0.0075 | −0.0017 | −0.0001 | 0.0003 | 0.0010 | −0.0005 | −0.0007 | −0.0014 |
| $b_6^4$ | −0.0144±0.0185 | −0.0345 | −0.0208 | −0.0140 | −0.0111 | −0.0150 | −0.0268 | −0.0106 |
| $n$ | 102 | 104 | 103 | 92 | 104 | 106 | 106 | 100 |
| $\chi^2$ | 0.1711 | 0.1683 | 0.2071 | 0.2632 | 0.0444 | 0.0990 | 0.2219 | 0.2352 |
| $\alpha$ | 0.24 ±0.06 | 0.26 | 0.28 | 0.34 | 0.21 | 0.22 | 0.24 | 0.29 |

TABLE IV. Values of SHP for $Gd^{3+}$-doped $LiY_{1-x}Yb_xF_4$ ($x=0.4$, 0.6, 0.8, 1.0). For notations see the caption of Table I.

| | $LiY_{0.6}Yb_{0.4}F_4$ | | | $LiY_{0.4}Yb_{0.6}F_4$ | $LiY_{0.2}Yb_{0.8}F_4$ | $LiYbF_4$ |
|---|---|---|---|---|---|---|
| $T$ (K) | 290 | 240 | 175 | 290 | 286 | 290 |
| $g_{zz}$ | 1.9782±0.0045 | 1.9790 | 1.9680 | 1.9852±0.0060 | 1.9762 | 1.9717 |
| $g_{xx}$ | 1.9867±0.0045 | 1.9894 | 1.9846 | 1.9964±0.0060 | 1.9916 | 1.9860 |
| $b_2^0$ | −2.4620±0.0145 | −2.4895 | −2.4954 | −2.4775±0.0165 | −2.4937 | −2.4812 |
| $b_4^0$ | −0.0601±0.0030 | −0.0566 | −0.0566 | −0.0601±0.0035 | −0.0645 | −0.0681 |
| $b_4^4$ | 0.3252±0.0075 | 0.3268 | 0.3402 | 0.3512±0.0090 | 0.3330 | 0.3209 |
| $b_6^0$ | 0.0016±0.0075 | 0.0027 | 0.0024 | −0.0009±0.0090 | −0.0001 | −0.0033 |
| $b_6^4$ | −0.0277±0.0185 | −0.0161 | −0.0157 | −0.0177±0.0210 | −0.0231 | 0.0108 |
| $n$ | 107 | 103 | 105 | 107 | 104 | 102 |
| $\chi^2$ | 0.2215 | 0.1890 | 0.3031 | 0.6297 | 0.6561 | 0.6298 |
| $\alpha$ | 0.26 ±0.06 | 0.25 | 0.30 | 0.25 ±0.07 | 0.30 | 0.33 |

$$\Delta E(T)=a'+b'T+c'T^2 \ . \tag{5.1}$$

The values of $a'$, $b'$, $c'$, and the corresponding $\chi^2$ values are included in Table V. The temperature dependence exhibited by Eq. (5.1) can be easily understood, if one takes into account the temperature dependence of the spin-Hamiltonian parameters $b_l^m$, as discussed in Sec. IV.

### B. Dependence on the mole fraction ($x$)

A reasonably good fit of $\Delta E$ values at room temperature can be made to the following quadratic function:

$$\Delta E(x)=29.6861-0.5273x+0.6062x^2 \ . \tag{5.2}$$

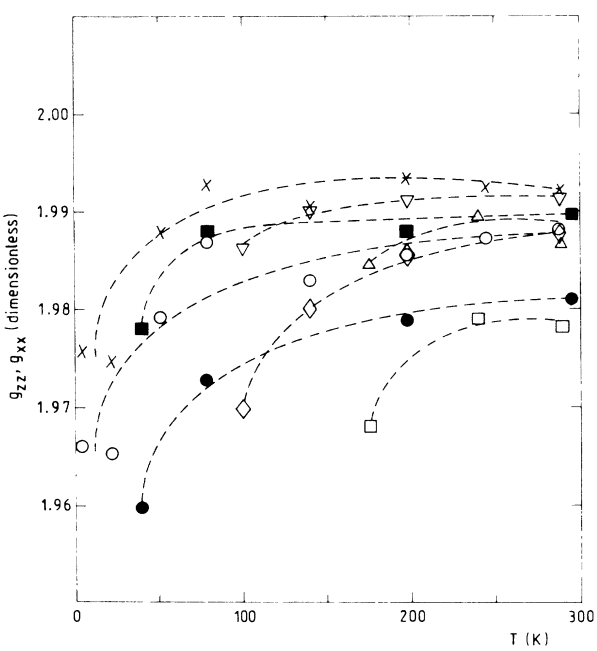


FIG. 5. Temperature variations of the $g$ values for the various hosts. The ($g_{zz}$,$g_{xx}$) values are represented by (○,×), (●,■), (◇,▽), and (□,△) for $LiY_{1-x}Yb_xF_4$; $x=0.1$, 0.2, 0.3, and 0.4, respectively.

The fit represented by Eq. (5.2) includes the values $x=0.0$, 0.1, 0.2, 0.3, 0.4, 0.6, 0.8, and 1.0, and is characterized by a $\chi^2$ value of 0.08 $GHz^2$.

## VI. SUPERPOSITION MODEL CALCULATION OF SHP ($b_l^m$)

According to the superposition model of Newman[6–8] the SHP ($b_l^m$) can be expressed as linear combinations of single-ligand contributions to the intrinsic parameters $\bar{b}_n(R_0)$, which depend on the ligand $i$, as follows:

$$b_l^m=\sum_i \bar{b}_n(R_i)K_n^m(\theta_i,\phi_i) \ , \tag{6.1}$$

where

$$\bar{b}_n(R_i)=\bar{b}_n(R_0)(R_0/R_i)^{t_n} \ . \tag{6.2}$$

In Eqs. (6.1) and (6.2), ($R_i,\theta_i,\phi_i$) are the coordinates of ligand $i$, and $R_0$ is a particular bond length, used as a reference. The $K_n^m$ in Eq. (6.1) are angular functions.[8] For the present considerations, they are specifically

$$K_2^0(\theta,\phi)=(3\cos^2\theta-1)/2 \ , \tag{6.3}$$

$$K_4^0(\theta,\phi)=(35\cos^4\theta-30\cos^2\theta+3)/8 \ , \tag{6.4}$$

$$K_4^4(\theta,\phi)=(35\sin^4\theta\cos 4\phi)/8 \ . \tag{6.5}$$

For $LiY_{1-x}Yb_xF_4$ crystals, one considers the eight ligand fluorines, which consist of four nearest and four next-nearest neighbors to a $Gd^{3+}$ ion, substituting a $Y^{3+}$, or $Yb^{3+}$ ion. This is shown in Fig. 3. The required values of ($R_i,\theta_i,\phi_i$) for $LiYF_4$ and $LiYbF_4$ are given in Refs. 11 and 16. In order to evaluate the intrinsic parameters, $\bar{b}_n(R_0)$, the required lattice constants of $LiY_{1-x}Yb_xF_4$ were estimated in accordance with Vegard's law,[12–14] as given in Sec. II. One can now express

$$\bar{b}_2(R_0)=b_2^0/[a(R_0/R_1)^{t_2}+b(R_0/R_2)^{t_2}] \ , \tag{6.6}$$

$$\bar{b}_4(R_0)=b_4^0/[c(R_0/R_1)^{t_4}+d(R_0/R_2)^{t_4}] \ , \tag{6.7}$$

$$\bar{b}'_4(R_0)=b_4^4/[e(R_0/R_1)^{t_4}+f(R_0/R_2)^{t_4}] \ . \tag{6.8}$$

TABLE V. Values of the constants required to fit the SHP: $b_l^m = a + bT + cT^2$ and the zero-field splitting: $\Delta E(T) = a' + b'T + c'T^2$. The $\chi^2$ values characterizing these fits are also included.

| | | $b_2^0$ | $b_4^0$ | $b_4^4$ | $\Delta E$ |
|---|---|---|---|---|---|
| $LiYF_4$ | $a'$ (GHz) | −2.6025 | −0.0598 | 0.3139 | 31.1166 |
| | $b'(10^{-5}$ GHz/K$^{-1})$ | 5.096 | 0.494 | 1.356 | −51.36 |
| | $c'(10^{-6}$ GHz/K$^{-2})$ | 1.232 | 0.082 | −0.158 | −15.04 |
| | $\chi^2(10^{-4}$ GHz$^2)$ | 0.16 | 0.002 | 0.03 | 23.5 |
| $LiY_{0.9}Yb_{0.1}F_4$ | $a'$ (GHz) | −2.5654 | −0.0591 | 0.3318 | 30.7032 |
| | $b'(10^{-4}$ GHz/K$^{-1})$ | −2.468 | −0.054 | −1.244 | 26.94 |
| | $c'(10^{-6}$ GHz/K$^{-2})$ | 1.887 | 0.048 | 0.167 | −21.95 |
| | $\chi^2(10^{-3}$ GHz$^2)$ | 0.26 | 0.005 | 0.1 | 31.4 |

In Eqs. (6.6)–(6.8), $R_1$ and $R_2$ are the distances of the nearest and next-nearest fluorine neighbors from the $Gd^{3+}$ ion, while $R_0 = (R_1 + R_2)/2$. As for the numerical values of the coefficients $a$, $b$, $c$, $d$, $e$, $f$, they are listed in Table VI for the various hosts. In the superposition-model calculation one needs to know the value of the power $t_n$ in Eq. (6.2). For $LiY_{1-x}Yb_xF_4$ crystals, which have the same crystal structure as those of Scheelite crystals, $t_2$ has been assumed to be equal to 1, which is the same as that used by Newman and Urban[8] for Scheelite hosts. A plot of $\bar{b}_2$ values as a function of $x$ at room temperature is displayed in Fig. 6. As for the value of $t_4$, it is determined from the condition $\bar{b}_4 = \bar{b}'_4$, where these intrinsic parameters are determined from the values of the parameters $b_4^0$ and $b_4^4$, using Eqs. (6.7) and (6.8), respectively. For $LiYF_4$ the values of $t_4$ turn out to be −58.8, −57.6, −57.3, and −57.1 at $T = 298$, 198, 140, and 93 K, respectively. This yields an average value of $t_4 = -57.8$ over the range 93–298 K. This value is, however, much greater in magnitude than those determined for $Gd^{3+}$-doped cubic-metal fluoride hosts $MeF_2$ (Me=Cd, Ca, Sr, Pb, Ba), for which $t_4 = -5.60$, −6.14, −4.86, −15.50, −7.43, respectively,[20] and for $Gd^{3+}$-doped hexagonal hosts $RF_3$ ($R$ =La, Ce, Pr, Nd), all of which have the same value of $t_4$ (=14).[21] The above-mentioned $t_4$ values for $LiY_{1-x}Yb_xF_4$ were, however, calculated without considering any distortions of the positions of $F^-$ ions, caused by the substitution of a $Gd^{3+}$ ion for $Y^{3+}$, or $Yb^{3+}$ ion; the latter ions do not have the same ionic radii as that of $Gd^{3+}$. In the absence of any knowledge of what these distortions are, some simple distortions were considered in order to see their effect on $t_4$. For example, reductions by the same value $\Delta\theta$ of all the eight vertical angles $\theta_i$ for the fluorine ions (Fig. 3); yield the $t_4$ values to be −21.3, −12.5, and −3.3 for $\Delta\theta$ equal to 4°, 5°, and 6°, respectively. This means that a reduction in the values of all $\theta_i$ by $\Delta\theta = 5.5°$ yields a $t_4$ value, which is consistent with those for $MeF_2$ (Ref. 20) and $RF_3$ hosts.[21]

## VII. TEMPERATURE DEPENDENCE OF THE INTRINSIC PARAMETER $\bar{b}_2$

The change in the value of $b_2^0$ with temperature can be reflected into the change in the value of the intrinsic parameter $\bar{b}_2$ with temperature. It has been suggested[17,22] that the effect of thermal expansion (contraction) of the lattice on $\bar{b}_2$ is rather small. Taking into account the change in lattice constants over the temperature range 93–290 K for $LiYF_4$,[9] the change in the value of $b_2^0$ is estimated, using Eq. (6.6), to be about 22%, while the total change in the value of $b_2^0$ as evaluated from experimental data is about 100%, which is much larger than 22%. The extra change in $b_2^0$ (about 78%), over and above that due to thermal change of lattice constants, can be explained to be due to the modulation of the crystal field by thermally excited phonons. The latter can be accounted for by the application of the isotropic Einstein model of lattice vibrations, according to which[23]

$$\bar{b}_2(T) = \bar{b}_2(RL) + K_2 \coth(\hbar\omega/2k_B T) . \quad (7.1)$$

In Eq. (7.1) $\hbar$ is Planck's constant divided by $2\pi$, $k_B$ is

TABLE VI. Values of the (dimensionless) coefficients $a$, $b$, $c$, $d$, $e$, $f$ required in Eqs. (6.6)–(6.8) for the various $LiY_{1-x}Yb_xF_4$ hosts.

| $x$ | $a$ | $b$ | $c$ | $d$ | $e$ | $f$ |
|---|---|---|---|---|---|---|
| 0.0 | −1.090 | 1.731 | −0.372 | −1.061 | 12.526 | 2.466 |
| 0.1 | −1.090 | 1.729 | −0.372 | −1.063 | 12.526 | 2.469 |
| 0.2 | −1.091 | 1.727 | −0.371 | −1.065 | 12.526 | 2.472 |
| 0.3 | −1.091 | 1.725 | −0.371 | −1.067 | 12.524 | 2.475 |
| 0.4 | −1.091 | 1.723 | −0.370 | −1.069 | 12.524 | 2.478 |
| 0.6 | −1.092 | 1.720 | −0.370 | −1.073 | 12.522 | 2.484 |
| 0.8 | −1.092 | 1.716 | −0.369 | −1.078 | 12.521 | 2.489 |
| 1.0 | −1.093 | 1.712 | −0.368 | −1.082 | 12.519 | 2.495 |

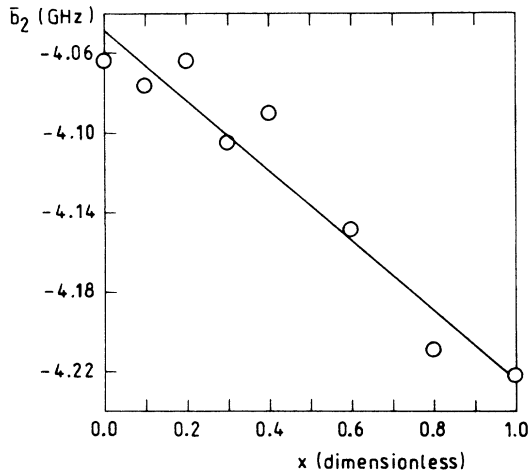


FIG. 6. Plot of the intrinsic parameter $\bar{b}_2(R_0)$ for $t_2=1$ as a function of $x$ at room temperature for the various $Gd^{3+}$-doped $LiY_{1-x}Yb_xF_4$ hosts.

Boltzmann's constant, and $\omega$ is the average frequency of phonons in the lattice of $LiYF_4$. Assuming a typical value of $\omega=10^{13}$ $s^{-1}$ for $LiYF_4$,[24] the values of $K_2$ and $\bar{b}_2(RL)$ are estimated, from a fit of $\bar{b}_2$ values to the temperature, according to Eq. (7.1), to be $K_2=0.0354$ GHz and $\bar{b}_2(RL)=-4.332$ GHz. The spin-phonon interaction constant $K_2$ can be calculated using the theory of vibronic effects.[25] Its magnitude is found to be proportional to $\langle u^2\rangle V_{OL}/R^2$, where $\langle u^2\rangle$ is the mean-square displacement of the atoms, $V_{OL}$ is the appropriate mean orbit lattice interaction energy, and $R$ is the rare-earth metal to fluorine distance. The value of $K_2$ as found here, from the fit to Eq. (7.1), is found to be of the same order of magnitude as that for $Eu^{2+}$-doped alkaline-fluoride crystals,[26] although $R$ for $LiYF_4$ is somewhat smaller than those for the alkaline-fluoride crystals.

## VIII. $Gd^{3+}$-$Yb^{3+}$ EXCHANGE INTERACTION

In this section the $Gd^{3+}$-$Yb^{3+}$ exchange-interaction constant, considering only the nearest and next-nearest neighbors, is estimated for the paramagnetic host $LiY_{0.9}Yb_{0.1}F_4$. To this end $\Delta g$, the shift of $Gd^{3+}$ $g$ value from that in the isostructural diamagnetic host $LiYF_4$ at liquid-helium temperature is used;[27] $\Delta g=g^p$-$g^d$, where $g^p$ and $g^d$ are the $g$ values in the isostructural paramagnetic ($LiY_{0.9}Yb_{0.1}F_4$) and diamagnetic ($LiYF_4$) hosts. (It is noted that the shape-dependent $g$ shift due to the magnetization of the $LiY_{0.9}Yb_{0.1}F_4$ sample at liquid-helium temperature[27,28] is zero in the present case, since the sample chosen for measurement was of spherical shape. As well, $LiY_{0.9}Yb_{0.1}F_4$ is the only mixed crystal for which EPR spectra can be recorded down to liquid-helium temperature.)

The spin-Hamiltonian of a $Gd^{3+}$-$Yb^{3+}$ pair can be expressed as follows:

$$\mathcal{H}_T=\mathcal{H}+\mathcal{H}'+\mathcal{H}_p \ . \tag{8.1}$$

The various terms on the right-hand side of Eq. (8.1) are described as follows. $\mathcal{H}$ is the spin-Hamiltonian of $Gd^{3+}$ ion in crystal field of tetragonal symmetry in $LiY_{0.9}Yb_{0.1}F_4$; it is given by Eq. (4.2).

$$\mathcal{H}'=\mu_B\mathbf{S}_1\cdot\tilde{g}_1\cdot\mathbf{H} \ , \tag{8.2}$$

is the spin-Hamiltonian of the $Yb^{3+}$ ion. In Eq. (8.2), $S_1=\frac{1}{2}$ is the effective spin of $Yb^{3+}$ in the ground state at liquid-helium temperature (see below), $\tilde{g}_1$ is the $g$ tensor for $Yb^{3+}$. [The hyperfine interaction energies of the two isotopes $^{171}Yb$ (nuclear spin $I=\frac{1}{2}$) and $^{173}Yb$ ($I=\frac{5}{2}$) with nonzero nuclear magnetic moments have been neglected.]

$$\mathcal{H}_p=J\mathbf{S}\cdot\mathbf{S}_1 \tag{8.3}$$

represents the $Gd^{3+}$-$Yb^{3+}$ pair-exchange interaction. In Eq. (8.3) $J$ is the exchange-interaction constant between a $Gd^{3+}$-$Yb^{3+}$ pair. The $g$ shift in a paramagnetic host from that in a diamagnetic isostructural host (in the present case $LiYF_4$) is expressed using the molecular-field model as[27,29]

$$\Delta g=zJ\langle\overline{\partial E_n/\partial H}\rangle/(g_1\mu_B^2H) \ . \tag{8.4}$$

In Eq. (8.4) $z$ is the number of nearest and next-nearest paramagnetic neighbor $Yb^{3+}$ ions to the $Gd^{3+}$ ion in $LiY_{0.9}Yb_{0.1}F_4$, $\langle\overline{\partial E_n/\partial H}\rangle$ is the average of the derivatives of the lowest-lying energy multiplet $^2F_{7/2}$ of $Yb^{3+}$ at liquid-helium temperature in $LiY_{0.9}Yb_{0.1}F_4$, and $g_1$ is the effective $Yb^{3+}$ $g$ factor. It should be noted that distant neighbors beyond the first nearest neighbors are not taken into account as the exchange-interaction constant falls off extremely rapidly with distance (for more details see Ref. 30).

$\langle\overline{\partial E_n/\partial H}\rangle$ can be calculated as follows. The $^2F_{7/2}$ level of $Yb^{3+}$ splits, in the presence of tetragonal crystalline electric field, into four Kramer's doublets $^2\Gamma_7+2^2\Gamma_8+^2\Gamma_9$;[31] however, at liquid-helium temperature only the ground-state doublet ($^2\Gamma_7$) is expected to be populated so that the effective spin of the $Yb^{3+}$ ion is $S_1=\frac{1}{2}$. Finally,

$$\langle\overline{\partial E_n/\partial H}\rangle=\sum_{i=1}^{2}(\partial E_i/\partial H)P_i \ , \tag{8.5}$$

where $E_1$, $E_2$ are the energies of the ground-state doublet of $Yb^{3+}$; $P_1$, $P_2$ are the corresponding probabilities of occupation. For $\mathbf{H}\|\hat{\mathbf{Z}}$, $E_1$ and $E_2$ can be expressed, using Eq. (8.2), as follows:

$$\begin{aligned} E_1&=-(g_{1z}\mu_BH)/2 \ , \\ E_2&=(g_{1z}\mu_BH)/2 \ . \end{aligned} \tag{8.6}$$

Assuming Boltzmann distribution the probabilities are

$$P_i=\exp(-E_i/k_BT)\Big/\sum_{i=1}^{2}\exp(-E_i/k_BT) \ , \tag{8.7}$$

where $E_i$ is given by Eqs. (8.6) and $k_B$ is Boltzmann's constant. Thus,

$$\langle\overline{\partial E_n/\partial H}\rangle=g_{1z}\mu_B(P_2-P_1)/2 \ . \tag{8.8}$$

Finally, the total exchange interaction between $Gd^{3+}$ and

its nearest and next-nearest paramagnetic $Yb^{3+}$ neighbors can be expressed, using Eq. (8.4), as

$$J' = zJ = 2(g_{zz}^p - g_{zz}^d)\mu_B H/(P_2 - P_1) \ . \tag{8.9}$$

Using $g_{1z} = 1.331$, $g_{1x} = 3.917$,[32] $H = 3400$ G as an average value for $X$-band EPR of $Gd^{3+}$, one finds $P_1 = 0.518$ and $P_2 = 0.482$ for $\mathbf{H} \| \hat{\mathbf{Z}}$, $P_1 = 0.553$ and $P_2 = 0.447$ for $\mathbf{H} \| \hat{\mathbf{X}}$, as calculated by the use of Eq. (8.7) at $T = 4.2$ K. Finally, one computes $J' = 6.3$ GHz using $\Delta g_{zz}$ while $J' = 1.3$ GHz using $\Delta g_{xx}$, in $Gd^{3+}$-doped $LiY_{0.9}Yb_{0.1}F_4$ single crystal. This yields the average value of $Gd^{3+}$-$Yb^{3+}$ pair-exchange interaction $J = 3.8 \pm 2.5$ GHz, averaged over the nearest and next-nearest neighbors, assuming that, on the average, there is one ($z = 1$) nearest and/or next-nearest $Yb^{3+}$ ion surrounding a $Gd^{3+}$ ion in the $LiY_{0.9}Yb_{0.1}F_4$ crystal. (It is noted that $z = 8$ for $LiYbF_4$.[33,34]) This value, estimated using the molecular-field model, taking into account the magnetization of the host $Yb^{3+}$ lattice,[27] is to be compared with $J = 8.60$ GHz, that obtained for $LiYbF_4$ at room temperature, using the model of Hutchings *et al.*[4]

## IX. CONCLUDING REMARKS

The present $X$-band EPR studies on $Gd^{3+}$-doped $LiY_{1-x}Yb_xF_4$ single crystals have led to the following conclusions.

(i) The various SHP in all $LiY_{1-x}Yb_xF_4$ exhibit the same, i.e., quadratic, dependence on temperature. This dependence is similar to that for $Gd^{3+}$-doped $LaAlO_3$ host.[19]

(ii) The $Gd^{3+}$ zero-field splittings (ZFS) depend quadratically on temperature, whereas in the $PrF_3$ (Ref. 35) and $Sm(NO_3)_3 \cdot 6H_2O$ (Ref. 36) hosts the $Gd^{3+}$ ZFS depend linearly upon temperature. Further, the present ZFS are about three times those in $PrF_3$ and $LaF_3$ hosts,[35] and $1\frac{1}{2}$ times that in the $Sm(NO_3)_3 \cdot 6H_2O$ host.[36]

(iii) The values of the same SHP for the various $LiY_{1-x}Yb_xF_4$ hosts are quite close to each other. This is the same behavior as that observed in the Scheelite host crystals. Newman and Urban[8] suggested that small variation in the observed parameters for different Scheelite crystals is caused by a rearrangement of the surrounding ions about the substituted ion, making the local environments in the various host crystals quite similar. In the present study, the substituting ions ($Gd^{3+}$) are larger than the host ions ($Y^{3+}$, $Yb^{3+}$); $Gd^{3+}$ ions, thus, push aside the ligand $F^-$ ions, forming local environments which could be quite similar in the various $LiY_{1-x}Yb_xF_4$ host crystals.

(iv) The variation of $b_2^0$ with temperature is predominantly due to the modulation of the crystal field by thermally excited phonons, i.e., due to spin-phonon interaction. The thermal expansion (contraction) of the crystal lattice plays a secondary role.

(v) The average $Gd^{3+}$-$Yb^{3+}$ exchange interactions with the nearest and next-nearest $Yb^{3+}$ ions in the $LiY_{0.9}Yb_{0.1}F_4$ host is estimated to be $3.8 \pm 2.5$ GHz at liquid-helium temperature, using the $g$ shift from that in the isostructural diamagnetic host $LiYF_4$.

(vi) The linewidth variation in $LiY_{1-x}Yb_xF_4$ hosts with larger $x$ values is very strongly temperature dependent, presumably due to $Gd^{3+}$-$Yb^{3+}$ dipole-dipole and exchange interactions. A detailed theoretical study of the temperature variation of the linewidths is in progress and will be published in due course.

## ACKNOWLEDGMENTS

The authors are grateful to the Natural Sciences and Engineering Research Council of Canada (Grant No. A4485) for partial financial support. One of us (L.E.M.) also acknowledges sponsorship by the Institute of Low Temperatures and Structural Research of Polish Academy of Sciences (programme CPBP-01.12.2.11—"Structure, phase transitions and properties of molecular systems and condensed phases").

*Permanent address: Department of Experimental Physics, Maria Curie-Sklodowska University, 20-031 Lublin, Poland.

[1]E. P. Chicklis and C. S. Naiman, IEEE J. Quant. Electron. **8**, 535 (1972).
[2]R. K. Watts and W. C. Holton, Solid State Commun. **9**, 137 (1971).
[3]Y. Vaills, J. Y. Buzaré, and J. Y. Gesland, Solid State Commun. **45**, 1093 (1983).
[4]S. K. Misra, M. Kahrizi, P. Mikolajczak, and L. Misiak, Phys. Rev. B **32**, 4738 (1985).
[5]S. K. Misra, J. Mag. Reson. **23**, 403 (1976).
[6]D. J. Newman and W. Urban, J. Phys. C **5**, 3103 (1972).
[7]D. J. Newman, J. Phys. C **6**, L271 (1973).
[8]D. J. Newman and W. Urban, Adv. Phys. **24**, 793 (1975).
[9]L. Misiak, P. Mikolajczak, and M. Subotowicz, Phys. Stat. Solidi A **97**, 353 (1986).
[10]R. E. Thoma, C. F. Weaver, H. A. Friedman, H. Insley, L. A. Harris, and H. A. Yakel, Jr., J. Phys. Chem. **65**, 1096 (1961).
[11]R. E. Thoma, G. D. Brunton, R. A. Penneman, and T. K. Keenan, Inorg. Chem. **9**, 1096 (1970).
[12]L. Vegard, Z. Phys. **5**, 17 (1921).
[13]L. Vegard, Z. Cryst. **67**, 239 (1928).
[14]S. K. Misra and P. Mikolajczak, Phys. Stat. Solidi B **109**, 59 (1982).
[15]A. Abragam and B. Bleaney, *Electron Paramagnetic Resonance of Transition Ions* (Clarendon, Oxford, 1970).
[16]X. Vishwamittar and S. P. Puri, J. Phys. C **7**, 1337 (1974).
[17]F. Mehran, K. W. H. Stevens, and T. S. Plaskett, Phys. Rev. B **20**, 1817 (1979).
[18]R. Lacroix, Helv. Phys. Acta **30**, 374 (1957).
[19]W. Low and A. Zusman, Phys. Rev. **130**, 144 (1963).
[20]J. Kuriata and W. Pastusiak, Acta Phys. Pol. A **66**, 627 (1984).
[21]S. K. Misra, P. Mikolajczak, and N. R. Lewis, Phys. Rev. B **24**, 3729 (1981).
[22]K. N. Shrivastava, Phys. Rep. C **20**, 137 (1975).
[23]S. B. Oseroff and R. Calvo, Phys. Rev. B **5**, 2474 (1972).

[24]S. A. Miller, H. E. Rast, and H. H. Caspers, J. Chem. Phys. **52**, 4172 (1970).
[25]J. M. Baker, J. Phys. C **12**, 4039 (1979).
[26]J. Kuriata, J. M. Baker, T. Rewaj, and N. Guskos, Phys. Stat. Solidi B **120**, K135 (1983).
[27]S. K. Misra and M. Kahrizi, Phys. Rev. B **37**, 5890 (1988).
[28]C. Kittel, Phys. Rev. **73**, 155 (1948).
[29]M. R. St. John and R. J. Myers, Phys. Rev. B **13**, 1006 (1976).
[30]S. K. Misra and S. Z. Korczak, Phys. Rev. B **35**, 4625 (1987).
[31]X. Vishwamittar, S. P. Taneja, and S. P. Puri, J. Phys. Chem. Solids **33**, 813 (1972).
[32]J. P. Sattler and J. Nemarich, Phys. Rev. B **4**, 1 (1971).
[33]S. K. Misra and J. Felsteiner, Phys. Rev. B **15**, 4309 (1977).
[34]L. M. Holmes, T. Johansson, and H. J. Guggenheim, Solid State Commun. **12**, 993 (1973).
[35]S. K. Misra, P. Mikolajczak, and S. Korczak, J. Chem. Phys. **74**, 922 (1981).
[36]S. K. Misra and P. Mikolajczak, J. Chem. Phys. **69**, 3093 (1978).